JOURNAL OF SYNCHROTRON RADIATION
ISSN 1600-5775

A refraction correction for buried interfaces applied to *in situ* grazing-incidence X-ray diffraction studies on Pd electrodes

Alan T. Landers,[a,b] David M. Koshy,[b,c] Soo Hong Lee,[d,e] Walter S. Drisdell,[d,e] Ryan C. Davis,[f]* Christopher Hahn,[b]* Apurva Mehta[f]* and Thomas F. Jaramillo[b,c,d]*

[a]Department of Chemistry, Stanford University, Stanford, CA 94305, USA, [b]SUNCAT Center for Interface Science and Catalysis, SLAC National Accelerator Laboratory, Menlo Park, CA 94025, USA, [c]Department of Chemical Engineering, Stanford University, Stanford, CA 94305, USA, [d]Joint Center for Artificial Photosynthesis, Lawrence Berkeley National Laboratory, Berkeley, CA 94720, USA, [e]Chemical Sciences Division, Lawrence Berkeley National Laboratory, Berkeley, CA 94720, USA, and [f]Stanford Synchrotron Radiation Lightsource, SLAC National Accelerator Laboratory, Menlo Park, CA 94025, USA. *Correspondence e-mail: rydavis@slac.stanford.edu, hahn31@llnl.gov, mehta@slac.stanford.edu, jaramillo@stanford.edu

Received 19 September 2020
Accepted 9 February 2021

Edited by V. Favre-Nicolin, ESRF and Université Grenoble Alpes, France

Keywords: grazing incidence X-ray diffraction; liquid–solid interfaces; *in situ* characterization; palladium; electrochemistry.

Supporting information: this article has supporting information at journals.iucr.org/s

In situ characterization of electrochemical systems can provide deep insights into the structure of electrodes under applied potential. Grazing-incidence X-ray diffraction (GIXRD) is a particularly valuable tool owing to its ability to characterize the near-surface structure of electrodes through a layer of electrolyte, which is of paramount importance in surface-mediated processes such as catalysis and adsorption. Corrections for the refraction that occurs as an X-ray passes through an interface have been derived for a vacuum–material interface. In this work, a more general form of the refraction correction was developed which can be applied to buried interfaces, including liquid–solid interfaces. The correction is largest at incidence angles near the critical angle for the interface and decreases at angles larger and smaller than the critical angle. Effective optical constants are also introduced which can be used to calculate the critical angle for total external reflection at the interface. This correction is applied to GIXRD measurements of an aqueous electrolyte–Pd interface, demonstrating that the correction allows for the comparison of GIXRD measurements at multiple incidence angles. This work improves quantitative analysis of *d*-spacing values from GIXRD measurements of liquid–solid systems, facilitating the connection between electrochemical behavior and structure under *in situ* conditions.

1. Introduction

In situ characterization of electrochemical systems allows researchers to relate the structure of electrodes during operation to their behavior (Choi *et al.*, 2017; Goonetilleke *et al.*, 2019). Spectroscopic, microscopic and scattering techniques have all been utilized to study the electronic and physical structure of electrodes in contact with an electrolyte (Choi *et al.*, 2017). Grazing-incidence X-ray diffraction (GIXRD) in particular has drawn interest for its ability to characterize the near-surface structure of electrodes, typically using high-intensity X-rays produced by synchrotron sources. Furthermore, by varying the incident angle of the incoming X-rays, the effective penetration depth of the X-ray can be controlled, enabling depth profiling measurements (Gibson, 2001; Kötschau & Schock, 2003; Dosch, 1992). Recent GIXRD experiments provided insight into electrocatalysis (Farmand *et al.*, 2019; Scott *et al.*, 2019; Higgins *et al.*, 2018; Escudero-Escribano *et al.*, 2018), corrosion (Scherzer *et al.*, 2019; De Marco *et al.*, 2007), ion selective electrodes (De Marco *et al.*,

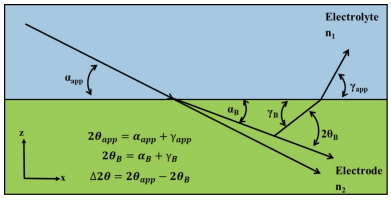

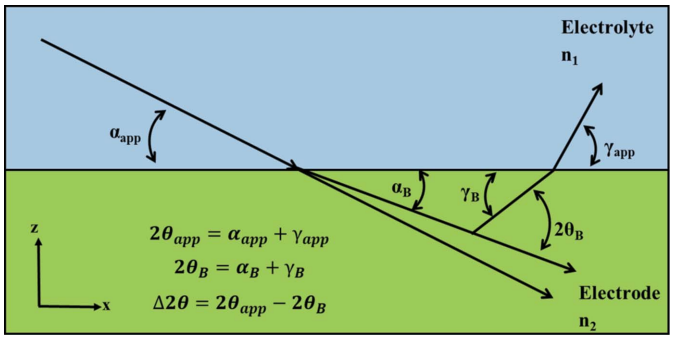

Figure 1
Geometry of the GIXRD experiments described in this work. For clarity, the magnitude of the refraction effect is exaggerated.

2006) and polymer layers on substrates (Busch *et al.*, 2006; Lee *et al.*, 2005) among other systems.

However, one of the challenges of using GIXRD to characterize electrodes under *in situ* conditions lies in the refraction of the X-rays. As the X-ray passes through the liquid–solid interface, its direction is altered as illustrated in Fig. 1. This refraction affects both the incoming and outgoing X-rays. If the real component of the index of refraction (δ) for the liquid is smaller than the real component of the index of refraction for the solid, as is typical for most water–solid interfaces at X-ray energies, the actual angle through which the X-rays are diffracted ($2\theta_B$) is smaller than the apparent diffraction angle ($2\theta_{app}$). This effect is well known in GIXRD, and corrections for this effect at vacuum–material interfaces (where the refractive index in a vacuum is defined to be one) have been developed (Toney & Brennan, 1989; Lim *et al.*, 1987; Liu & Yager, 2018; Busch *et al.*, 2006; Lee *et al.*, 2005; Breiby *et al.*, 2008). However, at liquid–solid interfaces, we must consider the value of the refractive index on both sides of the interface.

In this work, we develop a more general refraction correction which can be applied to a buried interface, including liquid–solid interfaces (*i.e.* electrolyte–electrode). We discuss the form of the correction and apply it to GIXRD measurements of an aqueous electrolyte–Pd interface. Lastly, we perform a simple sensitivity analysis, showing that the critical angle for the interface needs to be known to within a few hundredths of a degree to accurately correct for refraction. This correction enables the extraction of more quantitatively correct *d*-spacing values at multiple incidence angles corresponding to effective probe depths ranging from a few nanometres to bulk measurements.

2. Methods

GIXRD measurements were collected at Beamline 2-1 of the Stanford Synchrotron Radiation Lightsource at SLAC National Accelerator Laboratory with an incident energy of 17.0 keV (0.729 Å) and a Huber two-circle goniometer. The beam was slit down to a vertical height of ~30 µm and a nominal width of 1 mm. The scattered X-rays were measured using a Pilatus 100K area detector from Dectris with 487 × 195 pixels (172 µm × 172 µm pixel size). During measurements, the incident angle of the X-ray was fixed while the detector was moved through a range of diffraction angles.

The experimental details for collecting GIXRD measurements under electrochemical conditions have been described previously (Farmand *et al.*, 2019; Scott *et al.*, 2019). We deposited 50 nm Pd thin-film samples on an Si(100) substrate with a 3 nm Ti adhesion layer using an electron-beam physical vapor deposition system (Hahn *et al.*, 2015). We then mounted the sample in a custom 3D-printed electrochemical cell. Two platinum wires stretched above the sample serve as the counter electrode while an Ag/AgCl reference electrode is connected to the cell through a segment of tubing. During measurements, there is an approximately 500 µm layer of electrolyte over the sample. The electrolyte used in this study was a 0.10 *M* $K_xH_{3-x}PO_4$ buffer (pH ~6.8) that was continuously purged with Ar during measurements. The electrolyte was treated with a chelating agent (Chelex 100) to remove impurities. An HPLC pump was used to flow electrolyte over the sample during measurements.

Part of this derivation is described in the thesis of the lead author (Landers, 2020).

3. Results and discussion

To develop a correction for refraction at a liquid–solid interface, we utilize Snell's law to calculate the shift in the angle of the X-ray as it passes through the electrolyte–electrode interface (see the supporting information for the full derivation). The derivation generally follows the example by Toney & Brennan (1989) but does not make any simplifications for a vacuum–material interface. To this end, we define an effective index of refraction as follows,

$$n_{\rm eff} = \frac{n_2}{n_1} = \frac{1 - \delta_2 - i\beta_2}{1 - \delta_1 - i\beta_1}, \tag{1}$$

where n is the index of refraction for the material, δ is the real component of the index of refraction and β is the imaginary component of the index of refraction. Subscripts 1 and 2 refer to the liquid and solid side of the interface. As δ and β are $\ll 1$ within the X-ray energy range, we can approximate equation (1) to

$$n_{\rm eff} = 1 - \delta_{\rm eff} - i\beta_{\rm eff}, \tag{2}$$

where

$$\delta_{\rm eff} = \delta_2 - \delta_1 \tag{3}$$

and

$$\beta_{\rm eff} = \beta_2 - \beta_1. \tag{4}$$

Using equation (2) in Snell's Law and assuming that $\delta_{\rm eff}$ and $\beta_{\rm eff}$ are small but still result in observable refraction, we can now express the angle of the refracted incident X-ray using equation (5). In the derivation, we assume the angle of incidence is small enough for the small-angle approximation to be valid.

$$\alpha_{\rm B} = \left[\left(\alpha_{\rm app}^2 - 2\delta_{\rm eff} + \delta_{\rm eff}\,\alpha_{\rm app}^2\right) + i\left(\beta_{\rm eff}\,\alpha_{\rm app}^2 - 2\beta_{\rm eff}\right)\right]^{1/2}. \quad (5)$$

A related equation can be written for the refraction of the outgoing X-rays,

$$\gamma_{\rm B} = \left[\left(\gamma_{\rm app}^2 - 2\delta_{\rm eff} + \delta_{\rm eff}\,\gamma_{\rm app}^2\right) + i\left(\beta_{\rm eff}\,\gamma_{\rm app}^2 - 2\beta_{\rm eff}\right)\right]^{1/2}. \quad (6)$$

We can then calculate the shift in diffraction angle as shown in equation (7).

$$\begin{aligned}\Delta 2\theta &= 2\theta_{\rm apparent} - 2\theta_{\rm B} = \left(\alpha_{\rm app} + \gamma_{\rm app}\right) - \left(\alpha_{\rm B} + \gamma_{\rm B}\right)\\ &= \alpha_{\rm app} - \frac{1}{\sqrt{2}}\left\{\left[\left(\alpha_{\rm app}^2 - \theta_{c,\rm eff}^2 + \frac{\alpha_{\rm app}^2\,\theta_{c,\rm eff}^2}{2}\right)^2\right.\right.\\ &\quad \left.\left. + \left(-2\beta_{\rm eff} + \alpha_{\rm app}^2\beta_{\rm eff}\right)^2\right]^{1/2} - \theta_{c,\rm eff}^2 + \frac{\alpha_{\rm app}^2\theta_{c,\rm eff}^2}{2} + \alpha_{\rm app}^2\right\}^{1/2}\\ &\quad + \gamma_{\rm app} - \frac{1}{\sqrt{2}}\left\{\left[\left(\gamma_{\rm app}^2 - \theta_{c,\rm eff}^2 + \frac{\gamma_{\rm app}^2\theta_{c,\rm eff}^2}{2}\right)^2\right.\right.\\ &\quad \left.\left. + \left(-2\beta_{\rm eff} + \gamma_{\rm app}^2\,\beta_{\rm eff}\right)^2\right]^{1/2} - \theta_{c,\rm eff}^2 + \frac{\gamma_{\rm app}^2\theta_{c,\rm eff}^2}{2} + \gamma_{\rm app}^2\right\}^{1/2},\end{aligned} \quad (7)$$

where the effective critical angle, $\theta_{c,\rm eff}$, can be expressed as

$$\theta_{c,\rm eff}^2 = 2\delta_{\rm eff}. \quad (8)$$

Equation (7) shows that the magnitude of the correction depends on the incident and exit angles of the X-ray on the interface and the indices of refraction for the materials at the interface which are functions of material composition and X-ray energy.

Fig. 2 depicts the magnitude of the refraction correction calculated for an ideal water–Pd interface at 17.0 keV. The magnitude of the correction is greatest when the incidence or exit angles are close to the critical angle of the interface. As the incidence or exit angle of the X-ray increases, the magnitude of the correction decreases dramatically. The small refraction correction at large angles justifies why a correction is generally not utilized in non-grazing incidence XRD experiments. Furthermore, this behavior allows us to ignore the refraction correction for the outgoing X-ray if the exit angle is large compared with the critical angle. However, the refraction of the outgoing X-ray should not be ignored in small-angle X-ray scattering experiments, as shown in the small α and small γ region of Fig. 2. The derivation of equation (7) utilizes the small-angle approximation which shows a relative error of 1% at approximately 14° (0.24 radians). Thus, while equation (7) should be reasonably accurate within the range of angles shown in Fig. 2, its use to describe large diffraction angles would be inappropriate.

Here, we compare our work to a previously developed correction [equation (9)] (Toney & Brennan, 1989) for a vacuum–material interface whereby refraction of the outgoing X-ray was assumed to be negligible,

$$\Delta 2\theta = \alpha_{\rm app} - \frac{1}{\sqrt{2}}\left\{\left[\left(\alpha_{\rm app}^2 - \theta_c^2\right)^2 + 4\beta^2\right]^{1/2} - \theta_c^2 + \alpha_{\rm app}^2\right\}^{1/2}. \quad (9)$$

For the sake of direct comparison, we consider only the portion of equation (7) which describes the incident X-ray, and we simplify equation (7) to equation (10) accordingly,

$$\begin{aligned}\Delta 2\theta = \alpha_{\rm app} - \frac{1}{\sqrt{2}}&\left\{\left[\left(\alpha_{\rm app}^2 - \theta_{c,\rm eff}^2 + \frac{\alpha_{\rm app}^2\theta_{c,\rm eff}^2}{2}\right)^2\right.\right.\\ &\left.\left. + \left(-2\beta_{\rm eff} + \alpha_{\rm app}^2\beta_{\rm eff}\right)^2\right]^{1/2}\\ &- \theta_{c,\rm eff}^2 + \frac{\alpha_{\rm app}^2\theta_{c,\rm eff}^2}{2} + \alpha_{\rm app}^2\right\}^{1/2}.\end{aligned} \quad (10)$$

Equation (10) shows two key differences from equation (9). First, equation (10) uses an effective critical angle and index of refraction due to the impact of the liquid layer on refraction compared with the vacuum–material interface used in the construction of equation (9). Second, equation (10) adds higher-order terms that are not included in equation (9), multiplying the incidence angle by the critical angle or effective component of the refractive index. Since the critical and incidence angles are small, these higher-order terms contribute little to the overall magnitude of the correction compared

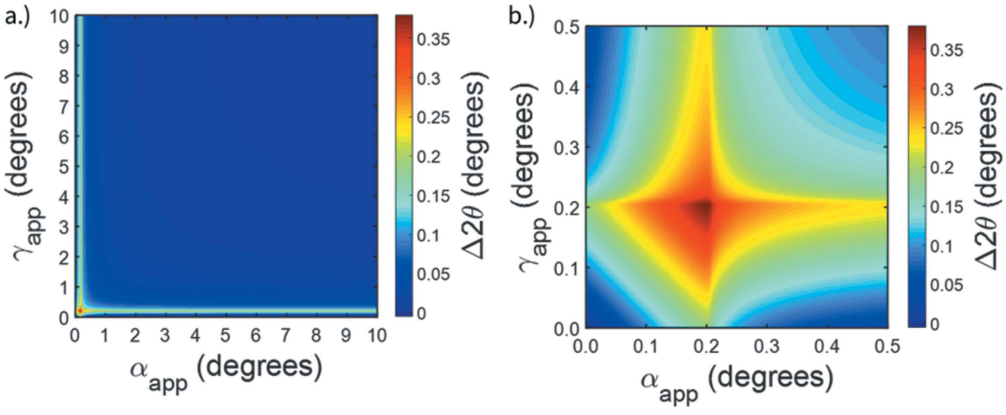

Figure 2
Magnitude of the refraction correction calculated for an ideal water–Pd interface at 17.0 keV using equation (7). Panels (*a*) and (*b*) display the same data with different axes values. The value of the effective critical angle is 0.207°.

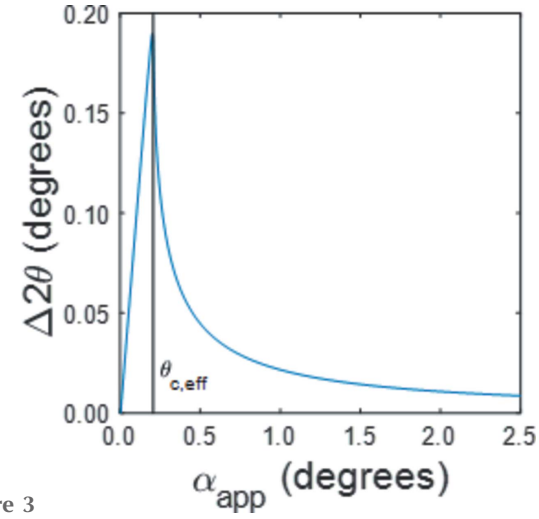

Figure 3
General form for the refraction correction calculated for an ideal water–Pd interface at 17.0 keV using equation (10). The value of the effective critical angle is 0.207°.

with that involving the impact of the liquid layer, and thus equation (10) can be reduced to equation (9) except for the use of values for the optical constant and the critical angle specific for the liquid–solid interface. Therefore, the two primary advances in this formulation of the refraction correction are the use of effective optical constants to describe a liquid–solid interface and the inclusion of the effect of refraction on both the incident and outgoing X-rays.

Fig. 3 displays the form of equation (10), which ignores the refraction of the outgoing X-rays, calculated for an ideal water–Pd interface at 17.0 keV. At incident angles below the critical angle, the value for the correction appears to increase linearly with the incident angle, reaching a maximum near the effective critical angle – the angle below which X-rays undergo total external reflection at the liquid–solid interface. At and below the critical angle, α_B is effectively zero, and the X-ray propagates as an evanescent wave just below the surface of the material (Gibson, 2001). At incident angles larger than the critical angle, the value of the correction decreases non-linearly as the incident angle increases.

In Fig. 4, we apply this refraction correction to GIXRD measurements of an aqueous 0.1 *M* $K_{3-x}H_xPO_4$–Pd interface held at +0.9 V versus reversible hydrogen electrode (RHE). Since the exit angle of the diffracted X-ray is large, we ignore the refraction of the outgoing X-ray. Fig. 4(*a*) shows GIXRD measurements collected at six different incidence angles. The peak positions are clearly shifted in the as-collected data. Since the incidence angle in GIXRD is related to the probe depth of the X-ray (Gibson, 2001), this observation could lead to the erroneous conclusion that the *d*-spacing of Pd varies as a function of depth. However, after applying equation (10), the diffraction peaks for all six angles closely match as shown in Fig. 4(*b*), demonstrating that the *d*-spacing of Pd is consistent as a function of depth.

Finally, Fig. 5 presents a sensitivity analysis of the refraction correction using equation (10). We plot the peak center for each GIXRD measurement after correcting for refraction

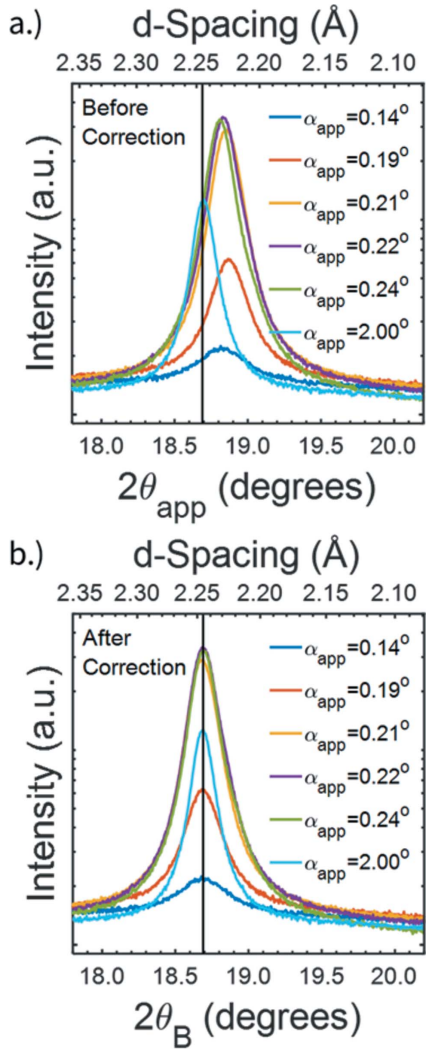

Figure 4
GIXRD measurements of a Pd thin-film electrode held at +0.9 V versus RHE in a 0.1 *M* $K_{3-x}H_xPO_4$ aqueous electrolyte (pH ∼6.8). (*a*) GIXRD measurements as collected, (*b*) correction of the measurements for refraction using equation (10) applied to an ideal H_2O–Pd interface.

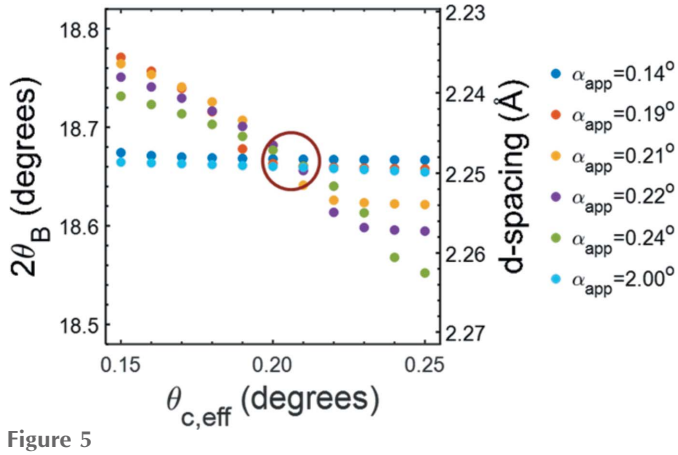

Figure 5
Peak centers for GIXRD measurements of a Pd thin-film electrode held at +0.9 V versus RHE in a 0.1 *M* $K_{3-x}H_xPO_4$ aqueous electrolyte corrected for refraction using various values for the effective critical angle. The red circles show the value of the effective critical angle where the peak positions appear to converge.

using different values for the effective critical angle. The red circle marks where the peak positions appear to converge near the calculated value for the ideal H_2O/Pd interface. This analysis demonstrates that the critical angle needs to be known to within a few hundredths of a degree to accurately correct the measurements for refraction. Fig. 5 also highlights the utility of equations (7) and (10) in that the correction can be performed using either a calculated value for the ideal interface or an experimentally measured critical angle.

We have developed a correction for the refraction that occurs as X-rays pass through a liquid–solid interface in GIXRD experiments. The correction depends on the angle of incidence and the optical properties of the material on both sides of the interface. We introduce effective optical constants which can be used to calculate the critical angle for total external reflection at the interface. Use of effective optical constants and the effective critical angle allows these more general equations to be reduced to a form identical to that in use for a vacuum–matter interface. The magnitude of the correction is largest near the critical angle for the interface and decreases at higher and lower incidence angles. It is also very sensitive to the critical angle for the interface, which must be either measured accurately or calculated if the optical constant for the liquid and the solid are precisely known. We have applied our correction to GIXRD measurements of an aqueous electrolyte–Pd interface, showing that our correction accurately describes the physics involved. This correction allows for the extraction of more accurate *d*-spacing values from GIXRD measurements and should aid in the study of electrocatalytic materials, battery systems and other liquid–solid interfaces.

Acknowledgements

We would also like to thank Charles Troxel Jr, Robert Tang-Kong, Samuil Belopolskiy, Valery Borzenets, Risa Benwell, Grace Tang, Matthew Padilla and Cathy Knotts for their support at SSRL.

Funding information

This material is based on work performed by the Joint Center for Artificial Photosynthesis, a DOE Energy Innovation Hub, supported through the Office of Science of the US Department of Energy (award No. DE-SC0004993). Use of the Stanford Synchrotron Radiation Lightsource, SLAC National Accelerator Laboratory, is supported by the US Department of Energy, Office of Science, Office of Basic Energy Sciences (contract No. DE-AC02-76SF00515).

References

Breiby, D. W., Bunk, O., Andreasen, J. W., Lemke, H. T. & Nielsen, M. M. (2008). *J. Appl. Cryst.* **41**, 262–271.
Busch, P., Rauscher, M., Smilgies, D.-M., Posselt, D. & Papadakis, C. M. (2006). *J. Appl. Cryst.* **39**, 433–442.
Choi, Y.-W., Mistry, H. & Roldan Cuenya, B. (2017). *Curr. Opin. Electrochem.* **1**, 95–103.
De Marco, R., Jiang, Z.-T., John, D., Sercombe, M. & Kinsella, B. (2007). *Electrochim. Acta*, **52**, 3746–3750.
De Marco, R., Jiang, Z.-T., Martizano, J., Lowe, A., Pejcic, B. & van Riessen, A. (2006). *Electrochim. Acta*, **51**, 5920–5925.
Dosch, H. (1992). *Critical Phenomena at Surfaces and Interfaces.* Berlin, Heidelberg, New York: Springer-Verlag.
Escudero-Escribano, M., Pedersen, A. F., Ulrikkeholm, E. T., Jensen, K. D., Hansen, M. H., Rossmeisl, J., Stephens, I. E. L. & Chorkendorff, I. (2018). *Chem. Eur. J.* **24**, 12280–12290.
Farmand, M., Landers, A. T., Lin, J. C., Feaster, J. T., Beeman, J. W., Ye, Y., Clark, E. L., Higgins, D., Yano, J., Davis, R. C., Mehta, A., Jaramillo, T. F., Hahn, C. & Drisdell, W. S. (2019). *Phys. Chem. Chem. Phys.* **21**, 5402–5408.
Gibson, P. N. (2001). *Encyclopedia of Materials: Science and Technology*, edited by K. H. J. Buschow, R. W. Cahn, M. C. Flemings, B. Ilschner, E. J. Kramer, S. Mahajan & P. Veyssière. Elsevier.
Goonetilleke, D., Stansby, J. H. & Sharma, N. (2019). *Curr. Opin. Electrochem.* **15**, 18–26.
Hahn, C., Abram, D. N., Hansen, H. A., Hatsukade, T., Jackson, A., Johnson, N. C., Hellstern, T. R., Kuhl, K. P., Cave, E. R., Feaster, J. T. & Jaramillo, T. F. (2015). *J. Mater. Chem. A*, **3**, 20185–20194.
Higgins, D., Wette, M., Gibbons, B. M., Siahrostami, S., Hahn, C., Escudero-Escribano, M., a, García-Melchor, M., Ulissi, Z., Davis, R. C., Mehta, A., Clemens, B. M., Nørskov, J. K. & Jaramillo, T. F. (2018). *ACS Appl. Energy Mater.* **1**, 1990–1999.
Kötschau, I. M. & Schock, H. W. (2003). *J. Phys. Chem. Solids*, **64**, 1559–1563.
Landers, A. T. (2020). PhD thesis, Stanford University, USA.
Lee, B., Park, I., Yoon, J., Park, S., Kim, J., Kim, K.-W., Chang, T. & Ree, M. (2005). *Macromolecules*, **38**, 4311–4323.
Lim, G., Parrish, W., Ortiz, C., Bellotto, M. & Hart, M. (1987). *J. Mater. Res.* **2**, 471–477.
Liu, J. & Yager, K. G. (2018). *IUCrJ*, **5**, 737–752.
Scherzer, M., Girgsdies, F., Stotz, E., Willinger, M.-G., Frei, E., Schlögl, R., Pietsch, U. & Lunkenbein, T. (2019). *J. Phys. Chem. C*, **123**, 13253–13262.
Scott, S. B., Hogg, T. V., Landers, A. T., Maagaard, T., Bertheussen, E., Lin, J. C., Davis, R. C., Beeman, J. W., Higgins, D., Drisdell, W. S., Hahn, C., Mehta, A., Seger, B., Jaramillo, T. F. & Chorkendorff, I. (2019). *ACS Energy Lett.* **4**, 803–804.
Toney, M. F. & Brennan, S. (1989). *Phys. Rev. B*, **39**, 7963–7966.